A&A manuscript no.
(will be inserted by hand later)
Your thesaurus codes are:
(07.36.1; 03.10.1; 09.14.1)

ASTRONOMY
AND
ASTROPHYSICS
5.8.1996

Galactic cosmic ray propagation: self-consistent models for nuclei, electrons and gamma rays

Submitted 5 Aug 1996

A.W. Strong[1], **and G.Youssefi** [1]

[1] Max-Planck Institut für extraterrestrische Physik, Giessenbachstrasse, Postfach 1603, 85740 Garching, FRG

[the date of receipt and acceptance should be inserted later]

Abstract. We describe a numerical approach to modelling the diffusive propagation of cosmic-ray nuclei and electrons in the Galaxy. Our main motivation is the interpretation of diffuse Galactic γ-ray emission. The model addresses both the spatial and energy dependence of the cosmic-ray distribution, uses the observed distribution of interstellar gas and radiation fields, and serves as the basis for predictions of γ-ray diffuse emission over the energy range 1 MeV - 10 GeV, non-thermal radio emission and the directly measured local interstellar electron spectrum. The cosmic-ray nuclear composition data sets tight constraints on the parameters of such models, and we require our models to be in accord with these. Electrons and nuclei are treated in a consistent way in the propagation code. The principal free parameter is the halo scale height, and a range of values 3 - 10 kpc is considered.

For a model with a constant electron injection spectrum it is not possible fit all the data within better than a factor 2. Since the deviations are significant the electron injection spectrum has been adjusted to fulfill better all the constraints set by the observations. This is shown to require a steepening of the injection spectrum by $\approx$0.4 in the index around a few GeV, since propagation effects alone cannot produce the required electron spectrum, at least within the confines of this diffusion model. For the model with a break the fit is improved overall, with the exception of γ-rays above 1 GeV, where too little intensity is predicted and other effects must be invoked. The model with break enables the steepening of the non-thermal radiation spectrum and the interstellar electron spectrum implied by recent studies of solar modulation of electrons to be simultaneously explained.

In order to improve predictions of the inverse Compton component, the interstellar radiation field over the Galaxy is recomputed ; this is of particular importance for the far-IR radiation field. Predictions of the high-latitude γ-ray spectrum including inverse Compton are presented which are of relevance to the derivation of the isotropic extragalactic component.

Key words: gamma rays: general; cosmic rays; interstellar medium :general

1. Introduction

We address the modelling of observational material related to cosmic-ray propagation in the Galaxy. The *main* motivation for this work is the interpretation of the diffuse Galactic γ-ray data from CGRO, but it is of relevance to a range of other astrophysical topics, in particular cosmic-ray electrons and the nature of cosmic-ray propagation in the Galaxy. We introduce a numerical approach to spatial Galactic cosmic-ray propagation which allows more realistic models than previous work which has been dominated by analytical methods. Electrons are of interest not only from the high-energy astrophysics viewpoint but also as a probe of the interstellar medium and propagation characteristics, since their spectrum is so strongly influenced by energy losses. The extension of the determination of the electron spectrum down to MeV energies via γ-ray astronomy is also proving important for *in situ* studies of propagation in the heliosphere in particular by the Ulysses spacecraft (Rastoin et al. 1996). For gamma-ray astronomy, the high-quality CGRO data on the diffuse emission from EGRET (Hunter et al. 1995,1996, Digel et al. 1995, Strong and Mattox 1996), COMPTEL (Strong et al. 1994, 1996) and OSSE (Purcell et al. 1996) require models which contain as much independent astrophysical input as possible. Such predictions serve as a reference, and can be used to evaluate how far the standard model of cosmic-ray propagation can go towards reproducing the observations.

The procedure we adopt is to construct a few 'standard models' using parameters which are plausible based on simple calculations or other studies. One or two steps of fine-tuning may then be performed to get a better representation of the data. Our aim is not a perfect fit but to obtain reasonably consistency with a whole range of observational material.

Another important goal is to produce model predictions of the inverse Compton γ-ray intensity spectrum as a function of direction, which can be used in analysis of the diffuse Galactic emission and also to evaluate the high-latitude intensity which affects the determination of the isotropic extragalactic background.

The spatial and energy dependent cosmic-ray propagation problem has traditionally been approached by analytical techniques, but the complexity of the calculations for models with the currently justifiable degree of realism now makes a numerical treatment preferable; surprisingly this approach has not been previously described in the literature, to our knowledge. Classical 'leaky-box' type composition calculations have no spatial component but follow cosmic-ray composition with a detailed reaction network, which is necessary for detailed composition studies. In contrast we treat the composition very simply, considering only B/C and ^{10}Be/Be , since this is sufficient for our purpose.

For previous work on this subject we mention Bloemen et al. (1993) who used an analytical treatment of the 2-D (R,z) problem for stable and radioactive secondaries, including convection not energy losses. Webber, Lee and Gupta (1992) also used an analytical method to solve the 2-D case, however without explicit inclusion of energy dependence. These studies are important as the first attempts to confront models which include a cosmic-ray gradient with the γ-ray and composition data simultaneously, and the results have been used to infer the halo size from more recent ^{10}Be/Be measurements (e.g. Lukasiak et al. 1994). Neither of these treatments was extended to electrons. The most extensive analytical treatments of electrons are by Lerche and Schlickeiser (1981, 1982a,b) which cover quite general cases including convection effects but include only one spatial dimension (z) and so ignore radial gradients which are important for a realistic model. Webber (1993) computed secondary nuclei and the electron spectrum in a self-consistent way for a leaky-box model; our work represents an extension of this approach to the spatial domain. Owens and Jokipii (1977) and van der Walt (1990) have used a Monte Carlo approach for electrons in one spatial dimension; this method is in principle even more flexible than our numerical solution of the partial differential equation, but an extension to three spatial dimensions would have rather extreme computing requirements.

2. Description of the model

The generally accepted basis for describing cosmic-ray propagation in the Galaxy consists of injection by sources in the galactic disc followed by diffusive and convective propagation with escape at some boundary. Energy losses and the diffusion coefficient are dependent on energy and position. Diffusive reacceleration certainly also plays a role. Here we restrict the model to diffusive transport with diffusion coefficient indepdendent of position, to investigate how far this can reproduce the observational data. The numerical methods developed allow convection and diffusive acceleration to be included easily in future.

An important feature of our approach is that cosmic-ray nuclei and electrons are treated within the *same* framework, in particular the dependence of the diffusion coefficient on kinematic parameters (rigidity, velocity) is assumed to have the same form for both particle types. We assume free escape at a boundary at height z_h above the disc; z_h is the most important free parameter of the model.

2.1. Propagation equation

The diffusive cosmic-ray transport equation for nuclei or electrons is written in the form:

$$\partial\psi(\boldsymbol{r},E,t)/\partial t =$$

$$q(\boldsymbol{r},E) + \nabla.[D\nabla\psi\ ] + \frac{\partial}{\partial E}[\psi\frac{dE}{dt}] - \frac{\psi}{\tau_i} - \frac{\psi}{\tau_r} \qquad (1)$$

where D is the diffusion coefficient and τ_i, τ_r are inelastic loss and radioactive decay times. The coordinate system used is (R,z,E) which assumes cylindrical symmetry of all quantities. Here R,z are Galactic radius and distance from the plane, and E is kinetic energy (for nuclei, kinetic energy per nucleon). This equation is solved by a time-dependent scheme starting from zero density until equilibrium is reached. For secondaries, the primary distribution is first computed, and then used in combination with the interstellar gas distribution and cross-sections to obtain the source term for secondaries, and the secondaries are then propagated in the same manner. The inelastic loss term is $\tau_i^{-1} = \beta c(\sigma_{p,H}n_H+\sigma_{p,He}n_{He})$. The secondary source function is $q_s(\boldsymbol{r},E) = \psi_p\beta c(\sigma_{ps,H}n_H(\boldsymbol{r}) + \sigma_{ps,He}n_{He}(\boldsymbol{r}))$; details of the cross-sections are given in section 8. The radioactive decay term is $\tau_r = [(1 + E_k/mc^2)/ln2]\tau_o$ where τ_o is the rest-frame half-life of the nucleus. The source function is assumed constant in time in this application, although the method would be equally applicable for a time-dependent source. In this work a convective term has not been included, but could easily be in future analyses. Details of the numerical method are given in the Appendix. For nuclei the solution is straightforward and fast. The main difficulty in the numerical solution in the case of electrons is the wide range of energy-loss time scales, ranging over 10^3 - 10^8 years for 1 MeV - 1000 GeV electrons. Here the solutions require considerable computer time for runs covering a wide energy range, even with the optimized method described in the Appendix.

The calculations are done on a grid with resolution 1 kpc in R and 0.1 kpc in z, reflecting the characteristic scales of variation in the two dimension. For secondary production and energy losses the average density in each cell is computed on a finer grid. The energy scale is logarithmic with a factor 1.2 between points.

2.2. Standard model parameters

In general terms, the stable secondary-to-primary ratio (e.g. B/C) fixes z_h/D while the radioactive secondary-to-primary ratio ^{10}Be/Be determines z_h^2/D (see e.g. Bloemen et al. 1993).

The cosmic-ray source distribution, the distribution of interstellar matter and energy losses combine to produce the observed values of these ratios. In principle both z_h and D are then determined but the quality of the ^{10}Be data is not yet sufficient to allow better than wide constraints on the parameters separately. We take two plausible values of z_h , 3 and 10 kpc, for our standard models, covering the range suggested by many other studies of nuclei and galactic synchrotron radiation (e.g. Phillipps et al 1981; Beuermann et al. 1985; Bloemen et al. 1993; Lukasiak et al. 1994).

The diffusion coefficient is assumed to depend on velocity βc and rigidity ϱ as $D(\varrho) = \beta D_o$ for $\varrho < \varrho_o$ and $D(\varrho) = \beta D_o(\varrho/\varrho_o)^\delta$ for $\varrho > \varrho_o$; studies of cosmic-ray nucleon secondary composition (Webber et al. 1996; Lukasiak et al. 1994) imply δ = 0.6 and ϱ_o = 3-5 GV. * For the source distribution q($\boldsymbol{r}$) we use the distribution of γ-ray emissivity (>100 MeV) determined from EGRET data by Strong and Mattox (1996) for R<15 kpc and zero source density for R>15 kpc. *A priori* it would be appropriate to use the distribution of potential cosmic-ray sources such as SNR, but as will be shown later the published SNR distributions give a cosmic-ray gradient much too large to be compatible with the γ-ray data even for large halo models. Also, the SNR distribution is very poorly known due to the difficulty of correcting for selection effects; the same holds for pulsars. For this reason we prefer to regard the source distribution as a part of the model starting with the γ-ray distribution, and iterating if necessary to get agreement with the γ-ray -derived gradient.

The nucleon distribution is affected by Coulomb (at low energies) and inelastic losses which depend on the gas density, so that the higher gas density in the inner Galaxy tends to to reduce the gradient relative to the source spectrum.

The injection spectrum is assumed to be a power-law in momentum, as predicted by theories of diffusive shock acceleration (see e.g. Reynolds 1991): $q(p) \propto p^{-\gamma}$ so that the differential spectrum with respect to kinetic energy is $q(E_k) \propto p^{-\gamma} dp/dE \propto p^{-\gamma}(E_k + mc^2)/p$. The injection index is taken initially as γ = 2.4. The power spectrum of non-thermal emission in the north galactic hemisphere has a spectral index of α = 0.5 - 0.6 over the range 38-408 MHz (Lawson et al. 1987) corresponding to $\gamma = 2\alpha + 1 = 2.0 - 2.2$. Broadbent et al. (1989) favour an index 0.7 (γ=2.4) for 408 MHz - 5 GHz for the low-latitude Galactic component. Reich and Reich (1988) give 0.85 (γ=2.7) for the 408-1420 MHz index of the plane emission, steepening to 1.0 or more out of the plane. The injection index is not uniquely determined in this way since there is no frequency at which the electron spectrum is completely unaffected by energy losses, which cause a continuous curvature of the spectrum; our value is adopted as a trial starting point, subject to fine tuning if required. In fact we will show evidence for a *break* in the electron injection spectrum, which in turn complicates the relation to the radio data.

* For an alternative interpretation involving diffusive reacceleration see Heinbach and Simon (1995).

3. Interstellar gas distributions

3.1. Atomic hydrogen

The atomic hydrogen distribution is represented by the formula

$$n_{HI} = n_{HI}(R) exp\left(-ln(2)(z/z_o(R))^2\right)$$

where $n_{HI}(R)$ is taken from Gordon and Burton (1976) and z_o from Cox, Krügel and Mezger (1986) giving an exponential increase in the width of the HI layer outside the solar circle:

$$z_o = 0.25 \ kpc, \quad R < 10kpc$$

$$z_o = 0.083 \ \exp(0.11R) \ kpc, \quad R > 10kpc$$

3.2. Molecular hydrogen

The distribution of molecular hydrogen is taken from Bronfmann et al. (1988) using CO surveys:

$$n_{H_2} = n_{H_2}(R) exp\left(-ln(2)(z/z_o)^2\right)$$

with z_o = 70 pc. The adopted radial distribution of HI and H_2 is shown in Fig 1 .

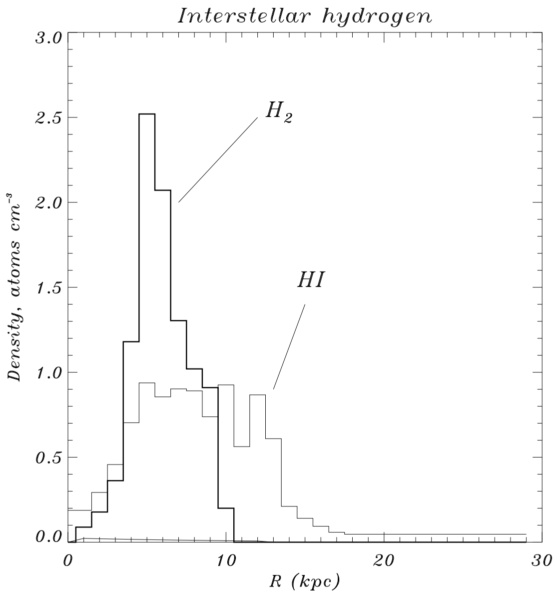

Fig. 1 . Adopted radial distributions of HI and H_2 density at z=0. Both distributions in atoms cm^{-3}

3.3. Ionized hydrogen

For the ionized gas we use the two-component model of Cordes et al. (1991) :

$$n_{HII} = 0.025 \ \exp\left(-\frac{|z|}{1.0kpc}\right) \exp\left(-\left(\frac{R}{20kpc}\right)^2\right)$$

$$+ 0.2 \ \exp\left(-\frac{|z|}{0.15kpc}\right) \exp\left(-\left(\frac{R-4}{2}\right)^2\right) \ cm^{-3}$$

The first term represents the extensive warm ionized gas and is similar to the distribution given by Reynolds (1989); the second term represents HII regions and is concentrated around R = 4 kpc. A temperature of 10^4 K is assumed to compute Coulomb energy losses in ionized gas.

4. Interstellar magnetic field

The magnetic field distribution is a major uncertainty and is treated as model-dependent with the criterion of consistency with non-thermal radio data. Heiles (1996) gives a value of 5μG for the random component and Rand and Lyne (1994) give $1.4\pm0.2\mu$G for the uniform component. We adopt $H_\perp$ = $6\exp(-z/z_{Ho})$ μG with z_{Ho}=5 kpc.

5. Interstellar radiation field

Several authors (Mathis et al. (1983), Chi and Wolfendale (1991), Bloemen (1985), Strong and Youssefi (1991)) have computed the ISRF over the Galaxy, but only Bloemen (1985) present the full (R,z,ν) distribution required for inverse-Compton calculations. We recompute the ISRF including new information in the mid- and far-IR from the IRAS surveys.

For the optical ISRF we follow previous work in using the four-component stellar population model of Mathis et al. (1983), performing line-of-sight integrations with absorption as a function of position from the same work and the absorption as a function of wavelength from Mathis et al. (1977). The absorption coefficient at $0.55\mu m$ for R=R$_o$ is taken as 0.46 mag kpc^{-1}.

There is considerable uncertainty in the radial scale-length of the stellar density; van der Kruit (1986) gives 5 kpc based on Pioneer 10 diffuse Galactic light observations, while Kent, Dame and Fazio (1991) give 3 kpc based on model fitting to $2.4\mu m$ surveys. While this and other new data (e.g. from COBE/DIRBE) could form the basis for a re-evaluation of this subject, this would be a major project and is not attempted.

The far IR calculation uses the emissivity distribution derived from an unfolding of IRAS data (Bloemen Deul and Thaddeus 1990).They give the FIR emissivity per HI and H_2 atom for 60 and 100 μm as a function of R; there is an increase in emissivity of about a factor 10 between the solar circle and the inner Galaxy, which is especially significant for the inverse-Compton component of γ-ray emission. The COBE/DIRBE analysis by Sodrowski et al. (1994) gives results in good agreement with Bloemen et al. and a dust temperature of 17-22K for the HI component and 19K for the H_2 component. We use a dust temperature of 24 K (Cox and Mezger 1989) and the HI, H_2 distributions given in Section 3. Figs 2 and 3 show the spectrum of the ISRF in the Galactic plane at R=5 kpc and 10 kpc, and Fig 4 shows the (R,z) distribution of the total density. Comparing our calculation with Mathis et al. (1983), the agreement is good in the optical range, confirming our calculation method, whereas in the FIR, where our model is based on IRAS results, we find significantly larger values especially in the inner Galaxy; a larger local FIR component was already noted from IRAS analyses (Cox and Mezger 1989).

For the range 8-50μm , which has not been considered before in this context, emission by PAHs and very small grains appears to be responsible for the diffuse radiation. Désert et al. (1990) constructed a detailed model for the specific emissivity per H atom in the solar neighbourhood. We use their Fig 4 and assume that the emissivity for HI and H_2 follows the same radial dependence as at $100\mu m$; the gas distribution again that of Section 3. This approximate procedure is sufficient since the ISRF in this range is less intense than at shorter and longer wavelengths.

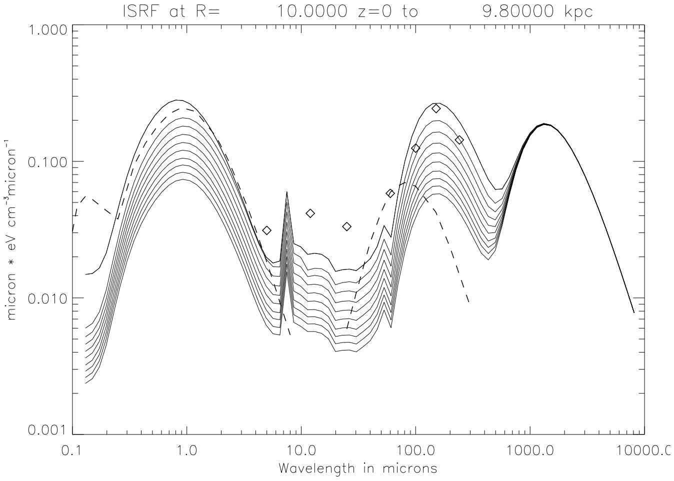

Fig. 2 . Spectrum of interstellar radiation at R = 10 kpc, z=0 to 10 kpc. The dashed curves are the calculations of Mathis et al. (1983) at R=10 kpc, z=0. The diamonds below $100\mu m$ are estimates given in Cox and Mezger (1989) based on IRAS data and $5\mu m$ data from Matsumoto et al. (1988). The diamonds at 151 and 241 μm are based on COBE/DIRBE results from Boulanger and Désert (1992), normalized to the $100\mu m$ IRAS point.

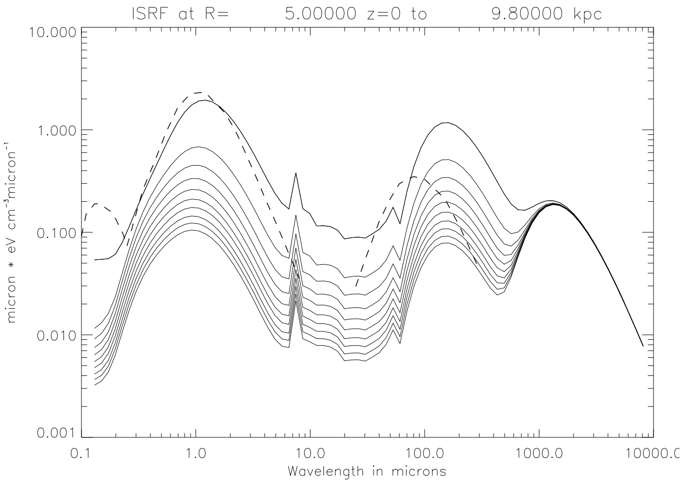

Fig. 3 . Spectrum of interstellar radiation at R = 5 kpc, z=0 to 10 kpc. The dashed curves are the calculations of Mathis et al. (1983) at R=5 kpc, z=0

Fig 4 shows the galactic ISRF energy density as a function of position; the rapid increase in the inner Galaxy is especially significant for the inverse Compton γ-ray emission. The full ISRF is available as a FITS file (see section 12).

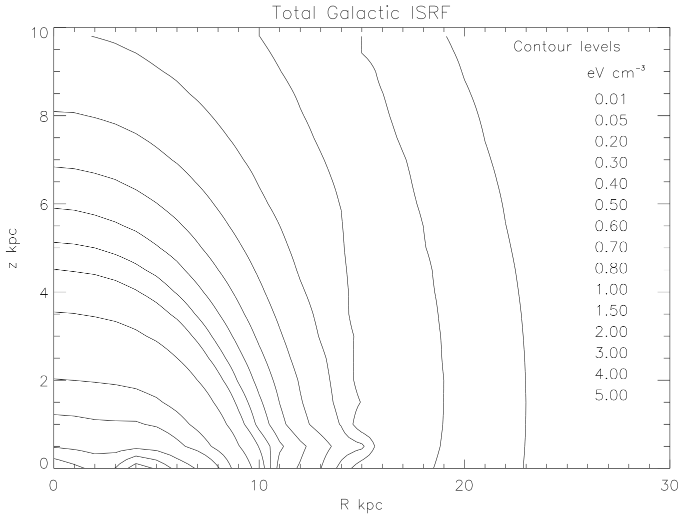

Fig. 4 . Energy density of Galactic interstellar radiation field (*not* including CMB, which contributes 0.24 eV cm^{-3} in addition).

6. Energy loss mechanisms

Although these processes are well known, for completeness we summarize here the formulae used; it is important to cover both non-relativistic and relativistic cases, losses on ionized gas and the contribution from He in the interstellar gas. The number density of He is assumed to be 0.11 times that of neutral H.

All formulae are in eV s^{-1}, and n is the appropriate target particle density in cm^{-3}.

6.1. Energy losses for electrons

6.1.1. Energy losses for electrons by ionization

For losses in neutral H and He we use the Bethe-Bloch formula in the form (see e.g. Skibo et al. 1996)

$$dE/dt = 7.6210^{-9}\ \frac{nZ}{\beta}(ln(1.38\ 10^9\gamma^2\beta^2 E_k)$$

$$-(\frac{2}{\gamma}-\frac{1}{\gamma^2})ln2+\frac{1}{\gamma^2}+\frac{1}{8}(1-\frac{1}{\gamma})^2)$$

For Coulomb losses on ionized H we use at ultrarelativistic energies. where plasma effects are important, (Ginzburg 1979 p 361: eq 15.24)

$$dE/dt = 7.62\ 10^{-9}\frac{n}{\beta}\left(73.4+ln(E/mc^2)-ln(n)\right)$$

At non-relativistic energies we use (Ginzburg 1979 p 363: eq 15.32)

$$dE/dt = 7.62\ 10^{-9}\frac{n}{\beta}\left(38.7+ln(E_k/mc^2)-\frac{1}{2}ln(n)\right)$$

6.1.2. Energy losses for electrons by bremsstrahlung

For losses on atomic H and He we use (Ginzburg 1979 page 386)

$$dE/dt = 5.1\ 10^{-10}nZ(Z+1)\frac{E_k}{mc^2}$$

and on ionized H

$$dE/dt = 7.0\ 10^{-11}n\frac{E_k}{mc^2}(ln\frac{E_k}{mc^2}+0.36)$$

6.1.3. Energy losses for electrons by inverse Compton

We use the simple formula for an isotropic radiation field assuming the Compton cross-section (Ginzburg 1979 page 386)

$$dE/dt = 2.64\ 10^{-14}W_{ph}\left(\frac{E_k}{mc^2}\right)^2$$

where W_{ph} is the radiation energy density in eV cm^{-3}

This is sufficient since the reduction due to the Klein-Nishina cross section affects only electrons of TeV energies interacting with $\approx$ 1 eV target photons.

6.1.4. Energy losses for electrons by synchrotron

$$dE/dt = 9.8\ 10^{-4}H_\perp^2\left(\frac{E_k}{mc^2}\right)^2$$

where $H_\perp$ is the perpendicular component of the magnetic field and we assume a random field such that $H_\perp^2 = \frac{2}{3}H^2$ (Ginzburg 1979 p. 386).

Fig 5 illustrates the contributions of all these loss processes for the local interstellar medium using our model.

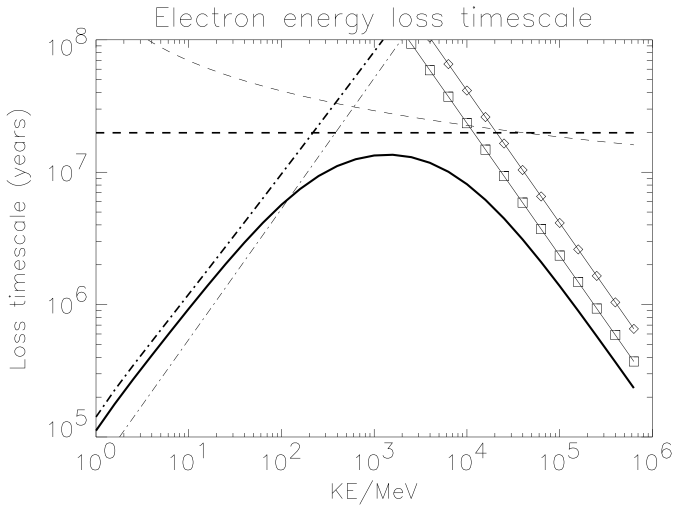

Fig. 5 . Energy loss timescales for electrons, illustrated for n_{HI}=n_{HII} = 1 cm^{-3}, $H_\perp$=6μG , W_{ph} =1 eV cm^{-3}. Thick, thin dashed lines: bremsstrahlung on neutral and ionized hydrogen; thick, thin dash-dot lines: Coulomb losses on neutral and ionized hydrogen; squares: synchrotron; diamonds: inverse Compton. Full thick line: total for same parameters except that n_{HII} = 0.1 cm^{-3}).

6.2. Energy losses for nuclei

A convenient summary of Coulomb energy losses of nuclei for all energies and for neutral and ionized media has been given by Mannheim and Schlickeiser (1994), and we refer to this paper for the detailed formulae. We use their equation (4.21) for neutral gas (H and He) and equation (4.22) for a warm ionized medium assuming a temperature of 10^4 K. Losses are especially important for cosmic-ray C, B etc. because of the Z^2-dependence of the loss rate. A typical loss time in the inner Galaxy is 10^6 years for C at 100 MeV/nucleon. This strongly affects the radial distribution of these cosmic rays at low energies, but has little influence at energies above 1 GeV/nucleon.

7. Gamma ray continuum production processes

7.1. Gamma ray production by bremsstrahlung

We consider only bremsstrahlung in the neutral interstellar medium, and use the formulae given by Koch and Motz (1959), including non-relativistic effects (Elwert factor). Screening by atomic electrons is treated following Blumenthal and Gould (1970). Bremsstrahlung on the extensive warm ionized interstellar medium may be of importance especially at high Galactic latitudes but in the galactic plane can be neglected in comparison to the combined contribution of atomic and molecular hydrogen, and helium.

7.2. Gamma ray production by inverse Compton

The inverse-Compton emissivity per unit volume and solid angle, ϵ_{ICS}, is computed using the Klein-Nishina cross-section for the case of an isotropic radiation field using (see e.g. Blumenthal and Gould 1970)

$$\epsilon_{ICS}(E_\gamma) = \frac{1}{c}\int\int \sigma_{ICS}(E_\gamma, E_e, \epsilon_{ph}) I(E_e) U(\epsilon_{ph}) dE_e d\epsilon_{ph}$$

where

$$\sigma_{ICS}(E_\gamma, E_e, \epsilon_{ph}) =$$
$$\frac{2\pi r_o^2}{\gamma^2 \epsilon_{ph}} \times \left(\frac{1}{2}(1-q)\frac{q^2\Gamma^2}{1+q\Gamma} + (1-q)(1+2q) + 2q\, ln(q)\right)$$

for

$$0 < E_\gamma < 4\gamma^2\epsilon_{ph}/(1+4\gamma\frac{\epsilon_{ph}}{m_e c^2})$$

with

$$\Gamma = \frac{4\gamma\epsilon_{ph}}{mc^2}, x = \frac{E_\gamma}{\gamma mc^2}, q = \frac{x}{\Gamma(1-x)}$$

$I(E_e)$ is the electron intensity and $U(\epsilon_{ph})$ is the differential photon density of the interstellar radiation field.

7.3. Gamma ray production by π^o -decay

We use the analytical formula given by Bertsch et al. (1994) based on the calculation of Stecker (1988). Unlike the electron component we do not base the gamma-ray production on the propagated cosmic-ray spectrum, but assume the spectral shape is constant thoughout the Galaxy. A fully self-consistent model using the propagated spectrum is left to future work, and demands attention particularly in view of the large deviation of the observed diffuse γ-ray spectrum from that predicted above 1 GeV (see Section 8).

7.4. Synchrotron radiation

We use the formula (Pacholcyk 1970, p. 90)

$$\epsilon_\nu(\nu) = 1.87\ 10^{-23} H_\perp \int \frac{4\pi}{c} I(E_e) f\left(\frac{\nu}{\nu_c}\right) dE_e$$

erg cm^{-3} sr^{-1} Hz^{-1} where $\nu_c = 6.27\ 10^{18} H_\perp E_e^2$ cgs,

The approximation

$$f\left(\frac{\nu}{\nu_c}\right) = 1.81\left(\frac{\nu}{\nu_c}\right)^{\frac{1}{3}} \exp\left(-\frac{\nu}{\nu_c}\right)$$

agrees with the exact formulae involving Bessel functions to within 10%.

8. Parameters and predictions of standard models

Two standard models with z_h = 3 and 10 kpc were studied. First the diffusion coefficient was adjusted to fit the B/C data for each model. The ^{10}Be/Be , cosmic-ray gradient, electrons and γ-rays were then computed, and compared with observations.

8.1. B/C and ^{10}Be/Be

We do not attempt a full reaction network but make approximations which allow the use of a single primary (^{12}C) solution to the diffusion equation. This approach similar to that used in the analytical analysis of Webber, Lee and Gupta (1992). This is sufficient for our purpose of constraining D and z_h. Nitrogen is 80% secondary (Gupta and Webber 1989) but can be treated as a progenitor in the B/C calculation by using observed relative abundance of N; the error introduced is negligible considering the N abundance is only about 12% of the other progenitors of B.

Table 1 summarizes the cross-sections used, including the sum of cross sections weighted by the observed abundances relative to Carbon in the galactic cosmic-rays. Cross sections are taken from from Gupta and Webber 1989 and Webber, Kish and Schreier (1990a,b,c) (see also Heinbach and Simon 1995). Relative abundances at 1 GeV are from HEAO, Englemann et al. (1990). Helium is included to sufficient accuracy by assuming primary-secondary cross sections on He a factor 1.3 larger than on H and destruction cross sections a factor 1.8 larger (Ferrando et al. 1988) and an 11% Helium abundance relative to

Table 1. Cross sections (in mb) used in this work. σ_p, σ_s: destruction of progenitor, secondary; σ_{ps}: progenitor $\rightarrow$ secondary. X$\rightarrow$B from Gupta and Webber 1989 (UNH values ^{10}B+ ^{11}B). X$\rightarrow$Be from Webber, Kish and Schrier (1990b: Table I) and (1990c: Table II). σ_p, σ_s from Webber, Lee and Gupta (1992: Table 1) and Webber, Kish and Schrier (1990a: Table IV) . Relative abundances at 1 GeV from HEAO, Englemann et al. (1990: Table 2). **Boldface values** are those finally used in the propagation calculation and allow for the presence of He in the ISM (see text).

Progenitor	Secondary	σ_p on H	σ_s on H	σ_{ps} on H	Relative abundance of progenitor (O=1000)
C	B	250	232	75.0	1089
N	B	252		46.5	319
O	B	308		37.7	1000
Ne	B			21.9	167
Mg	B			15.6	206
Si	B			10.3	158
weighted total for C $\rightarrow$B				131	
used for C $\rightarrow$B for H + He target			**290**	**151**	
B	Be		190	36.6	365
C	Be			13.9	
N	Be			13.7	
O	Be			12.8	
weighted total for C $\rightarrow$Be				42	
used for C $\rightarrow$Be for H + He target			**237**	**48**	
B	^{10}Be		212	5.0	
C				2.5	
N				1.6	
O				2.3	
weighted total for C $\rightarrow$ ^{10}Be				6.8	
used for C $\rightarrow$ ^{10}Be for H + He target			**265**	**7.8**	

hydrogen,giving a factor 1.14 in the secondary yields and 1.25 in the destruction rate. Energy losses are included as described in Section 6.

We require agreement with the B/C data above 1 GeV/nucleon where the solar modulation effect is minimal. For each z_h we adjust the magnitude of D_o to give an acceptable fit; we find values 2.0 10^{28} cm^2 s^{-1} for z_h = 3 kpc and 5.0 10^{28} cm^2 s^{-1} for z_h = 10 kpc. A break rigidity ρ_o = 3 GV was found satisfactory. The model B/C values as a function of energy are shown in Figs 7a and 7b . The B/C measurements are taken from Webber et al. (1996) (Voyager 1+2); a modulation of 500 MV was applied to the model spectra using the force-field approximation. As expected we do not fit the B/C data below 1 GeV since this would require either removing the β factor from the diffusion coefficient, which seems unphysical, or the inclusion of a convective term, or diffusive reacceleration (Heinbach and Simon 1995). However since fitting the low energy nuclear data is not the main motivation for the present study we have not attempted to tune the model in this region.

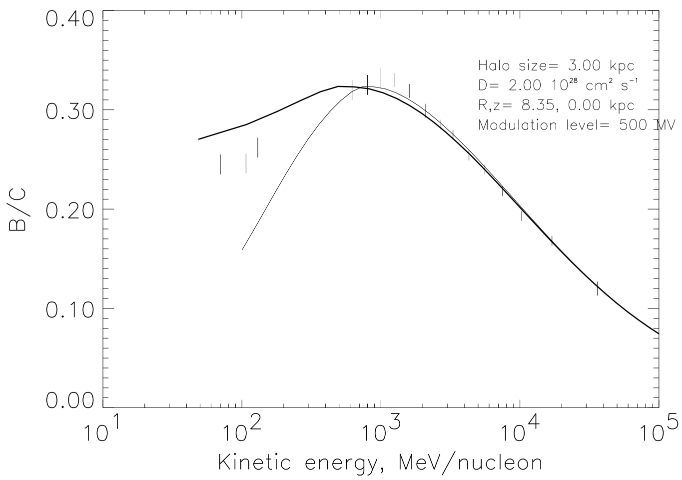

Fig. 7a . B/C for the standard model with z_h = 3 kpc, D_o = 2.0 10^{28} cm^2 s^{-1} . Data from Webber et al. (1996).

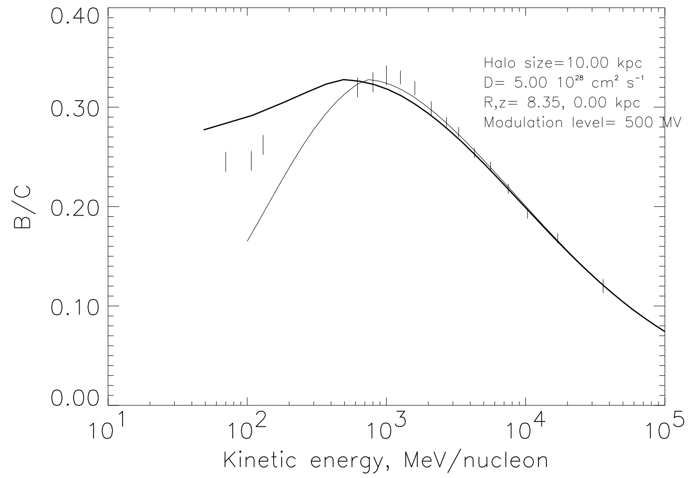

Fig. 7b . B/C for the standard model with z_h = 10 kpc, D_o = 5.0 10^{28} cm^2 s^{-1} . Data from Webber et al. (1996).

The ^{10}Be/Be ratio (Fig 8) is consistent with the observations for both z_h = 3 and 10 kpc. Lukasiak et al. (1994) give z_h = 2.8±1 kpc based on the same data and the analytical model of Webber, Lee and Gupta (1992), for the case of no convection. Since our model explicitly includes the observed distribution of gas and adjusts D to give the observed B/C for each z_h , it gives finally a more realistic result (within the confines of the model) than was possible with the analytical approach. We conclude that any z_h in the 3 - 10 kpc range is acceptable, and pending higher accuracy ^{10}Be/Be data more precise constraints must come from radio or γ-ray results or from the high-energy electron spectrum.

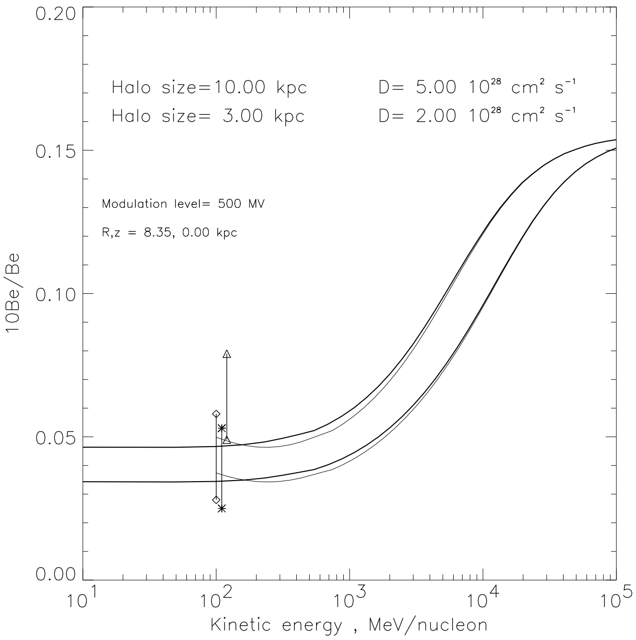

Fig. 8 . ^{10}Be/Be for the standard models with z_h = 3 and 10 kpc. Data from Lukasiak et al. (1994).

We can compare our results to the analytical solution of the 1D diffusion equation in z which gives a ‘grammage’ (see e.g. Bloemen et al. 1993)

$$\Lambda = 1.44 \frac{z_h N_H m_H \beta c}{2D} =$$

$$7.8\beta \, \frac{z_h}{kpc} \, \frac{N_h}{10^{21} cm^{-2}} \, / \, \frac{D}{10^{28} cm^2 s^{-1}} \; g \; cm^{-2}$$

where N_H is the integrated hydrogen column density of the disk in atom cm^{-2} which for our model is about 1.0 10^{21} cm^{-2}averaged over the inner Galaxy; the factor 1.44 allows for an assumed He fraction of 0.11. The most recent values obtained from detailed composition studies of the same data give Λ = 12.5β (Webber et al. 1996) at low rigidities (below 4 GV/nuc) so that $D_o = 0.62 z_h/kpc$ 10^{28} cm^2 s^{-1} , ie 1.9 and 6.2 10^{28} cm^2 s^{-1} for z_h = 3 and 10 kpc respectively. *

This calculation is approximate since it ignores the variation of gas density in the galaxy, energy losses etc. but serves as a useful check on the values (D_o = 2.0, 5.0 10^{28} cm^2 s^{-1}) from our numerical calculation; they are in good agreement. Our values can also be compared with the analytical diffusion model of Webber, Lee and Gupta (1992); they adopt D = 0.6 10^{28} cm^2 s^{-1} at 1 GV for a model with z_h = 2 kpc, corresponding to D_o = 1.2 10^{28} cm^2 s^{-1} . Since $D_o \propto z_h$ this value is quite consistent with ours.

8.2. Cosmic-ray nuclei gradients

The radial variation of CR nucleon intensity at z=0 is illustrated in Fig 6 for ^{12}C. At low energies it is strongly affected by Coulomb losses, with a minimum around R= 5 kpc where the gas density is largest; at high energies only the source distribution and diffusion affect the distribution.

* Note that $\Lambda \propto \beta$ is not actually consistent with diffusion since D itself should be proportional to β for a diffusive random-walk process, and this cancels the β in the above formula for Λ.

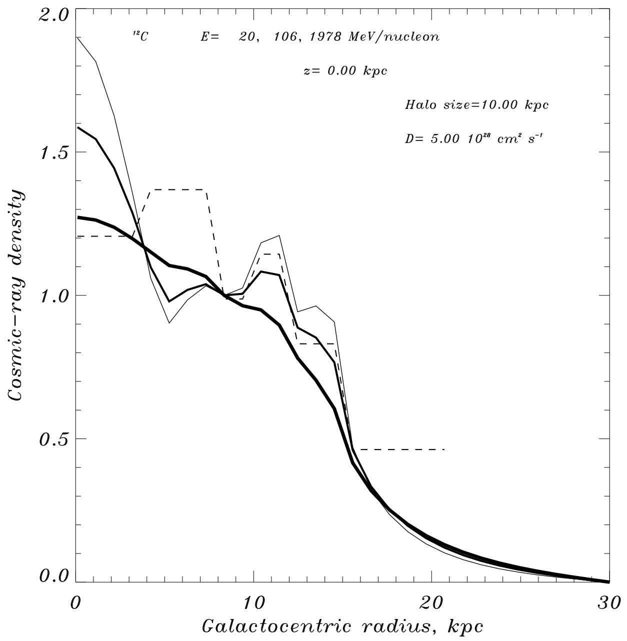

Fig. 6 . Radial variation of flux of CR nuclei at z=0 for model with z_h =10 kpc. ^{12}C is used to illustrate the effect of energy and fragmentation losses at low energies. Thin, medium,thick lines: 20, 106, 1978 MeV/nucleon. The dashed line is the variation of $>$100 MeV γ-ray emissivity from EGRET analysis (Strong and Mattox (1996); this is also the assumed distribution of cosmic-ray sources in this model, except for that we cutoff the source distribution at R = 15 kpc.

At high energies the distribution of CR nuclei is the same as for CR protons and hence should agree with the gradient derived from gamma-ray studies above a few 100 MeV. In Fig 6 we also show the gradient $>$100 MeV from the EGRET analysis of Strong and Mattox (1996) with the high-energy nucleon distribution. Since this was the form used for the source distribution it illustrates that the diffusive propagation has little effect on the gradient except to flatten it slightly. In any case our model satisfies the condition of generating a gradient consistent with that derived from γ-rays , and no attempt was made to fine-tune the source distribution. As mentioned in Section 2.1 the source gradient for R$<$R$_o$is much flatter than expected from published distributions of SNR or pulsars (see Strong 1996 for a detailed comparison), but these distributions are very uncertain due to large selection effects so that cosmic-ray origin in SNR is not necessarily inconsistent with our model.

8.3. Electrons

The latitude distribution of electrons over the range of energies for z_h = 3 and 10 kpc is illustrated in Figs 9 and 10 , for R=R$_o$. At low energies ionization losses in the extended gas layer cause a falloff relative to the linear falloff characteristic of diffusion from a plane source exhibited when there are small losses (around 1 GeV). At higher energies, synchrotron and inverse-Compton cause a steadily faster falloff.

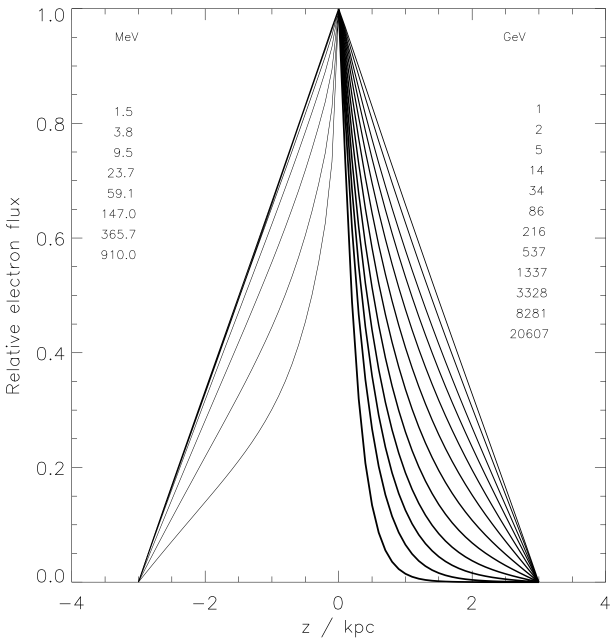

Fig. 9 . Electron flux as a function of z at R=R$_o$ for the standard model with z_h =3 kpc. Energies $<$1000 MeV, $>$1000 MeV shown at negative, positive z respectively,

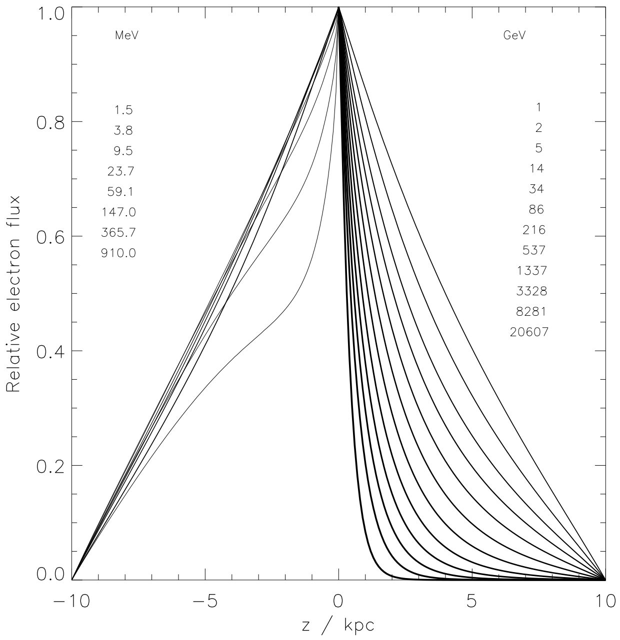

Fig. 10 . Electron flux as a function of z at R=R$_o$ for the standard model with z_h =10 kpc. Energies $<$1000 MeV, $>$1000 MeV shown at negative, positive z respectively.

The radial distribution at z = 0 is shown in Fig 11 for z_h = 10 kpc, for various energies. At energies below 10 MeV Coulomb losses cause the flux to be anticorrelated with the gas distribution as can be seen by comparison with Fig 1. This produces a dip in the flux around R = 5 kpc. The electron distribution is therefore a rapidly varying function of energy in R as well as z.

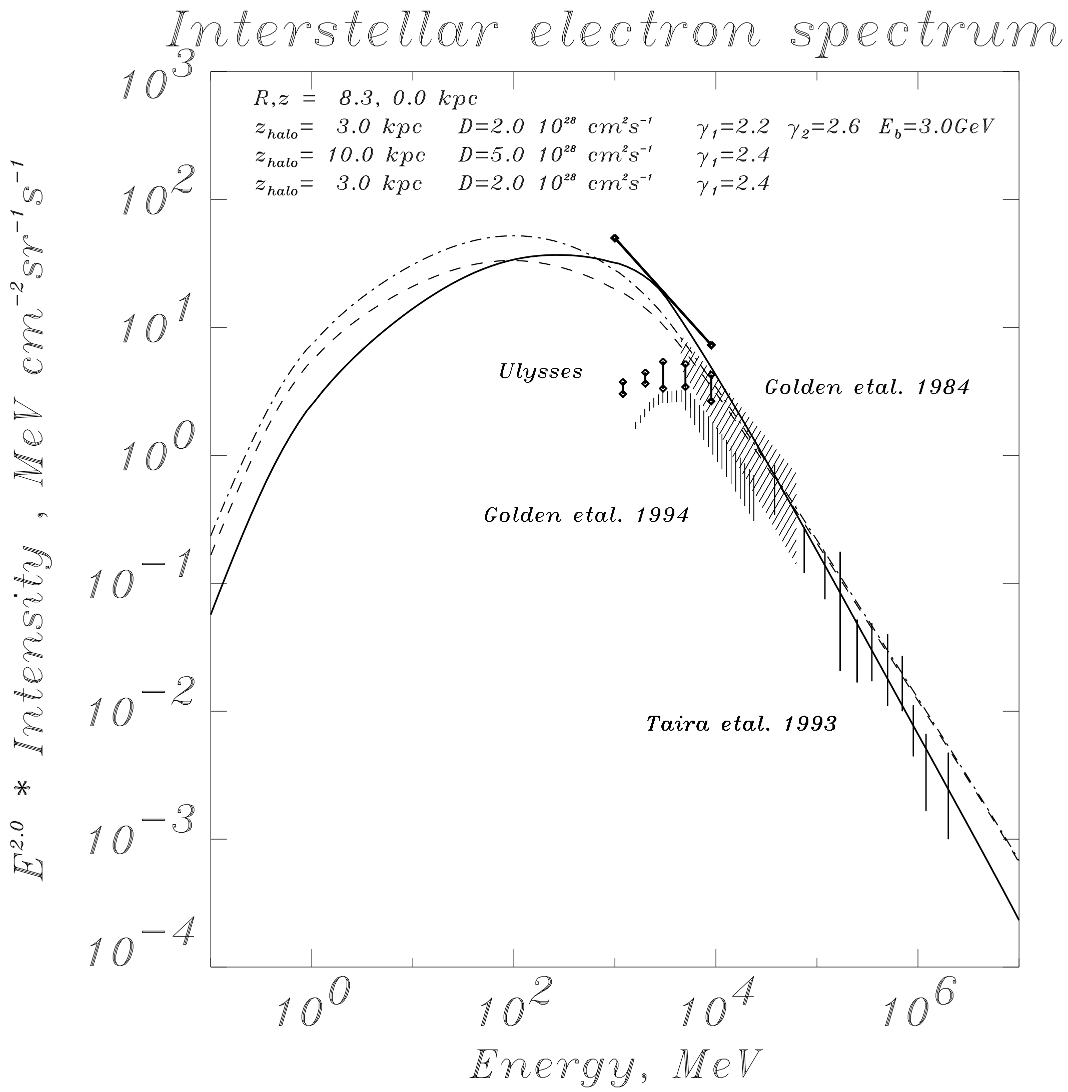

Fig. 12 . Electron spectrum at R=R_o for the standard models. The dashed and dashed-dot curves are for an electron injection spectrum with constant index -2.4, and are normalized to pass though the Ulysses measurement at 9 GeV . Dashed curve: z_h = 3 kpc, D_o = 2.0 10^{28} cm^2 s^{-1} ; dash-dot curve: z_h = 10 kpc, D_o = 5.0 10^{28} cm^2 s^{-1} . The full line is for an electron injection spectrum with a break from -2.2 below 3 GeV to -2.6 above 3 GeV, and z_h =3 kpc, Do=2.0 10^{28} cm^2 s^{-1} ; it is normalized to pass though the interstellar electron spectrum at 9 GeV based on heliospheric propagation modelling of Ulysses data. Data : shaded : Golden et al. (1984, 1994); vertical bars: Taira et al. (1993); diamonds + vertical bars :Ferrando et al. (1996): Ulysses, extreme southern heliographic latitude. Diamonds + sloping line: Ferrando et al. interstellar spectrum based on heliosphere propagation model.

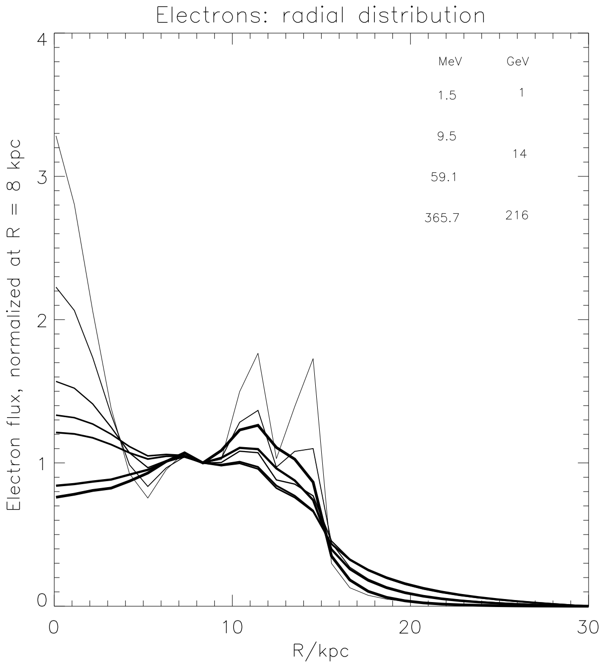

Fig. 11 . Electron profiles as as function of R at z=0 for the standard model with z_h =10 kpc. In order of increasing line thickness, energies are 1.5, 9.5, 59,366 MeV, 1, 14, 216 GeV.

The predicted electron spectrum in the local interstellar medium (R=R_o) is shown in Fig 12 . It is compared to direct measurements of electrons in the solar vicinity: observations up to 1 TeV from balloons (Taira et al. 1993; Nishimura et al. 1995; Golden et al. 1984, 1994), and the measurements up to 9 GeV by Ulysses at its southernmost heliographic latitude excursion (Ferrando et al. 1996). At energies above 5 GeV the solar modulation decreases and so we require our model to be consistent with the observed fluxes there. We have chosen to normalize our two standard models to the *observed* 9 GeV Ulysses flux; the model then reproduces the higher-energy balloon data up to 1 TeV, although the predictions are rather too high above 100 GeV. The most recent modulation models predict some significant modulation even at 10 GeV (Ferrando et al. 1996). If we wish to accomodate slightly higher flux at 9 GeV and at the same time fit the electron data up to 1 TeV, we require other adjustments in the model to maintain consistency with the high-energy electron and the low-energy γ-ray data; in Section 9 we propose the introduction of a break in the electron injection spectrum. The corresponding propagated electron spectrum is also plotted in Fig 12 .

8.4. Gamma Rays

8.4.1. Observations

For the energy range $>$30 MeV we use the spectrum derived from multicomponent fits to EGRET data (Strong and Mattox 1996). This analysis used full-sky EGRET datasets from CGRO Phase 1+2 together with HI and CO surveys including kinematic information to obtain the emissivity spectrum as a function of galactocentric radius. An inverse Compton model and catalogued sources were also included but unresolved source components were not modelled. The CO-to-H_2 scaling factor X_{CO} was a free parameter determined in the fitting. For the 1-30 MeV range we use the COMPTEL analysis (Strong et al. 1996) based on the same HI and CO data. The method was similar to that used for EGRET, but the COMPTEL data does not allow such a detailed gradient analysis. For comparison with the diffusion models we use (i) the local emissivity taken as the average for the two rings nearest the solar position, (ii) intensities averaged over a large region of the inner Galaxy and (iii) high-latitude intensities. The intensities are computed directly from the published multicomponent fits. The COMPTEL emissivity spectrum used is the average for the inner Galaxy rather than the local value (since no gradient analysis was possible); depending on the size of the gradient at these energies the plotted values may be up to a factor 1.5 too high and this must be borne in mind when making the comparison. OSSE measurements in the inner Galaxy are also available (Purcell et al. 1996; Strong et al. 1996), extending the data down to 50 keV.

8.4.2. Model vs. γ-ray observations

Figs 13a , 13b show the predicted local (R=R_o, z=0) γ-ray emissivity spectrum per gas atom (thus excluding the IC component). The agreement with the measurements within a factor 2 over 4 decades of energy is itself remarkable, but the deviations are nevertheless important. At high energies the discrepancy has already been noted (Hunter et al. 1996) and may indicate a contribution from unresolved γ-ray point sources or a dramatic difference in the proton spectrum enhancing the π^o-decay component at high energies; in any case it cannot be explained by any plausible modification to the electron spectrum. At low energies the COMPTEL points agree sufficiently well with the predictions, bearing in mind the uncertainties mentioned in section 8.4.1. For 30 - 100 MeV the prediction is about a factor 2 high relative to the EGRET measurement; however this is the most difficult EGRET energy range with the broadest point-spread function so that some systematic effects in the observed spectrum cannot be excluded.

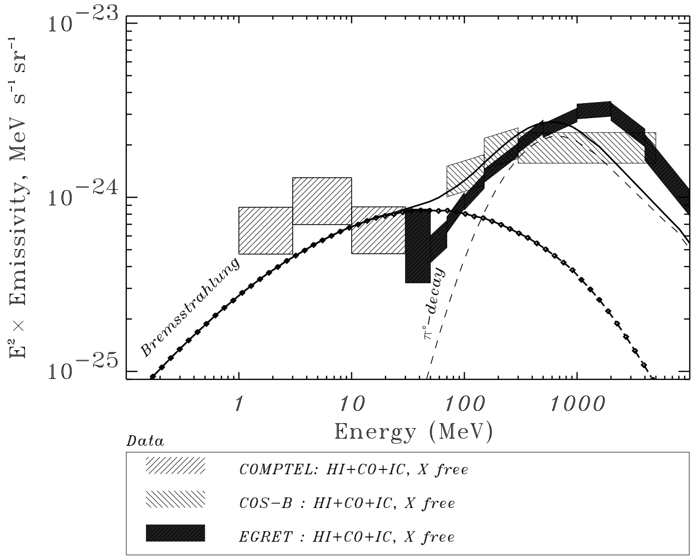

Fig. 13a . Gamma-ray emissivity spectrum for model with z_h = 3 kpc, D_o =2.0 10^{28} cm^2 s^{-1} . Data from Strong et al. (1996) (COMPTEL), Strong and Mattox (1996) (EGRET)

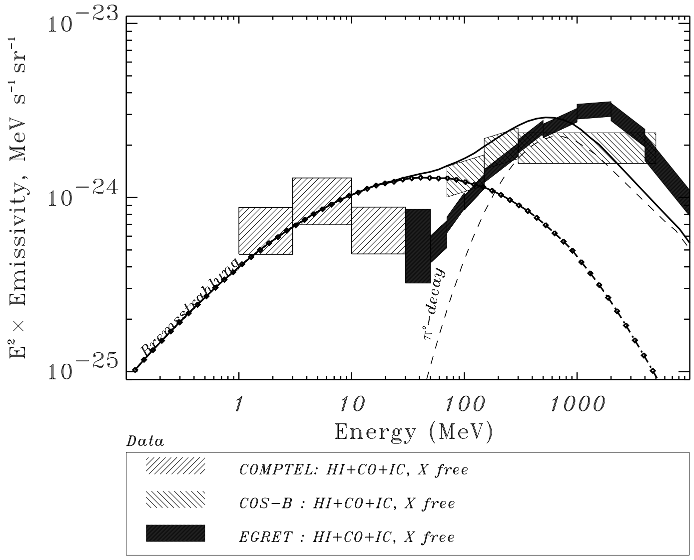

Fig. 13b . Gamma-ray emissivity spectrum for model with z_h = 10 kpc, D_o =5.0 10^{28} cm^2 s^{-1} . Data as Fig 13a

Figs 14 and 15 show the average intensity in the inner Galaxy, 300^o <l<60^o , |b| <20^o . The predicted bremsstrahlung and π^o intensities use the model emissivities q(R,z,E_γ) per gas atom combined with the gas column density for annuli in R based on HI and CO surveys, since this gives the most accurate representation of the gas distribution as seen from the solar vicinity (see Strong and Mattox 1996 for a description of the gas data). The IC predictions are obtained by integration of the volume emissivities over the line-of-sight. Again the predictions agree within a factor 2 with the data. Most interesting is the IC component which is about equal to the bremsstrahlung around 1-3 MeV and increases with the halo size. For the z_h = 10 kpc halo the IC is 20% of the total emission at 100 MeV, for the latitude interval shown.

Considering either the emissivity of intensity spectra, the optimal overall fit for $E_\gamma < 1$ GeV would be for a model with intermediate z_h , around 5 kpc. In no case can a good fit above 1 GeV be obtained.

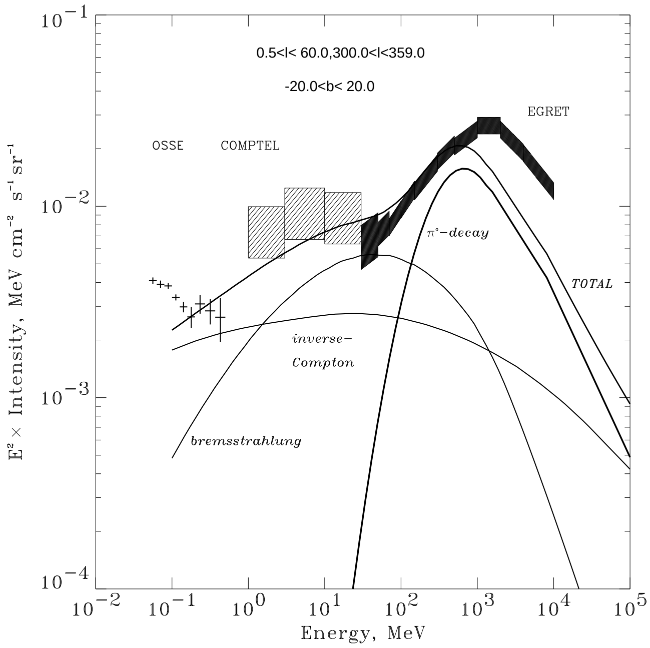

Fig. 14 . Gamma-ray intensity spectrum in the inner Galaxy, 300^o <l<60^o , |b| <20^o . z_h = 3 kpc, D_o =2.0 10^{28} cm^2 s^{-1} . Data points based on synthesis of multicomponent fits, references as for Fig 13a .

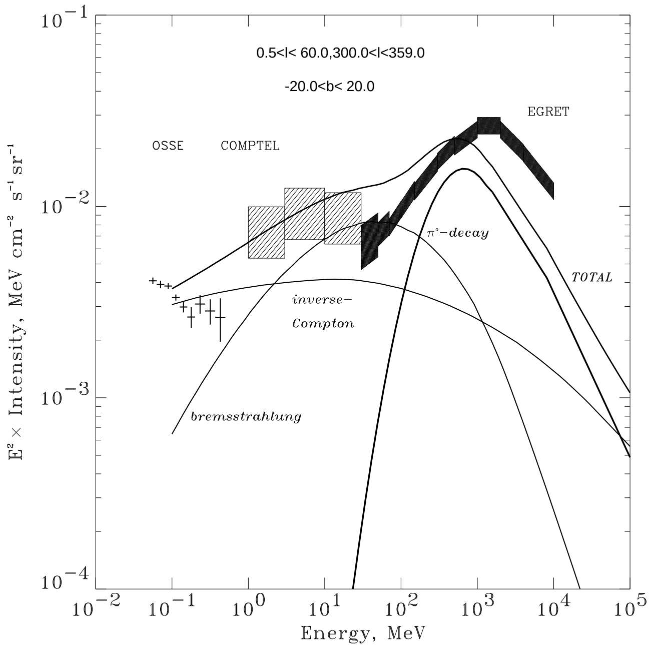

Fig. 15 . Gamma-ray intensity spectrum in the inner Galaxy, 300^o <l<60^o , |b| <20^o . z_h = 10 kpc, D=5.0$10^{28}$ cm^2 s^{-1} . Data as Fig 14 .

Figs 16 and 17 show intensities at high latitudes, 260^o <l<280, ^{o} 60^o <b<70^o , for z_h = 3 and 10 kpc respectively.

The IC emission now dominates below 100 MeV. For comparison the isotropic component from the EGRET analysis (Strong and Mattox 1996) and the *total* high-latitude diffuse emission from COMPTEL (Kappadath et al. 1996) for this sky region are shown. In the 10-30 MeV range the Galactic contribution to the high-latitude emission is about 30% for z_h = 3kpc and 50% for z_h = 10 kpc. This underlines the importance of the Galactic emission in evaluating the isotropic extragalactic background. The inverse Compton intensity prediction for z_h =10 kpc at high latitudes is large due to the big halo and has an intensity 40% of the isotropic component. However the predicted emission lies significantly above the EGRET Galactic intensity between 30 and 100 MeV and so is hardly compatible with the data. The largest halo compatible with (i.e. not exceeding) all the high-latitude γ-ray data would be for $z_h \approx 5$ kpc.

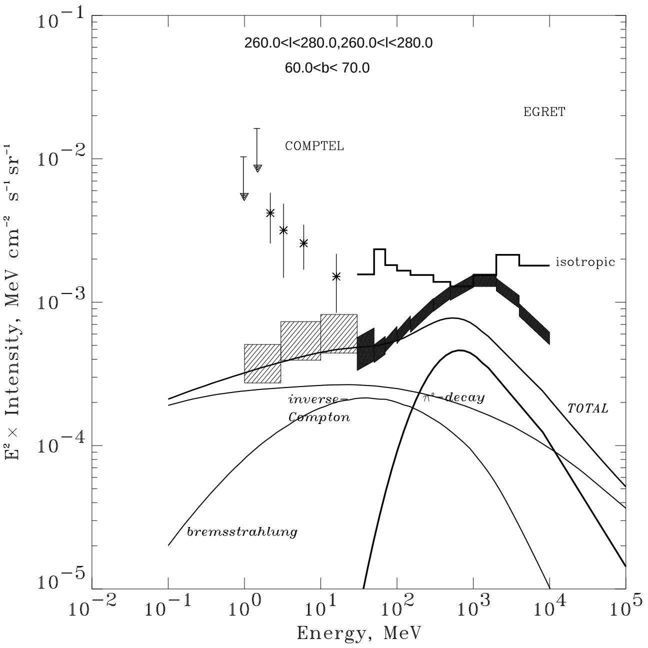

Fig. 16 . Gamma-ray intensity spectrum at high latitudes $260^o < l < 280^o$, $60^o < b < 70^o$. Model: z_h = 3 kpc, D_o =2.0 10^{28} cm^2 s^{-1} . The measured spectra are based on multicomponent fits to COMPTEL and EGRET data using the same model (Strong et al. 1996, Strong and Mattox 1996). The sum over the Galactic components (excluding isotropic emission) are shown. The high-latitude absolute total intensity from COMPTEL for this sky region (vertical bars: Kappadath et al. 1996) and the isotropic component from EGRET (histogram) are also shown.

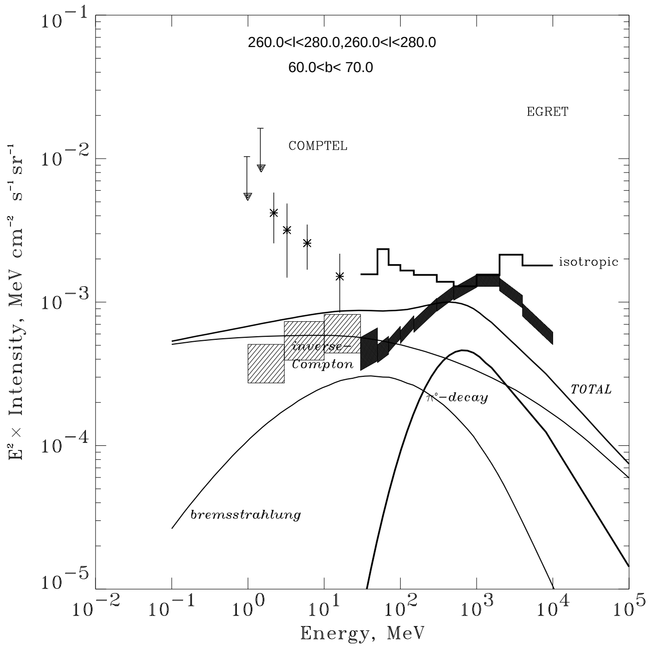

Fig. 17 . Gamma-ray intensity spectrum at high latitudes for model with z_h = 10 kpc, D_o = 5.0 10^{28} cm^2 s^{-1} . Data as in Fig 16 .

8.4.3. Energies below 1 MeV

There are indications from OSSE and Ginga of a sharp upturn at still lower energies based on the diffuse emission in the hard X-ray range (Purcell et al. 1996; Skibo et al. 1996; Yamasaki et al. 1996). We do not attempt to fit this rapid turnup in the spectrum below 1 MeV; it would require a rapid steepening of the injection spectrum for nonrelativistic electrons and is beyond the scope of the present work. A model which does reproduce the spectrum is given by Skibo et al. (1996). It is however not clear whether this radation is truly diffuse; a population of flat-spectrum hard X-ray sources could also be responsible.

8.5. Non-thermal radio

In Fig 18 we compare our predicted spectra at the Galactic pole with that derived from modelling the 408 MHz all-sky maps by Broadbent et al. (1990), who give a polar temperature of 12.3K for the Galactic component. The intensities at 38 MHz and 1420 MHz are plotted using published ranges in spectral index as explained in the caption and discussed in Section 2.2. The agreement of the absolute level within a factor 2 shows that our assumed $H_\perp$ distribution combined with our model electron distribution is at least reasonably consistent with the radio data. A slight increase of the field would give better agreement in the average radio intensity for the model with z_h = 3 kpc but otherwise would have only a minor affect on the model, increasing the synchrotron energy losses somewhat.

Our model spectrum is too steep below 408 MHz, on account of our electron spectral index of -2.4, and the change of slope around 408 MHz poses a problem for a model with constant injection index; it does not seem possible to produce the observed steepening by propagation and energy losses alone. The shape of non-thermal spectrum suggests a break in the electron spectrum around 3 GeV for a 5μG field; this is supported by the independent considerations given in the section 9. Fig 18 shows also the spectrum for the model with a break at injection from -2.2 to -2.6 at 3 GeV, showing how the fit is improved in this case. *

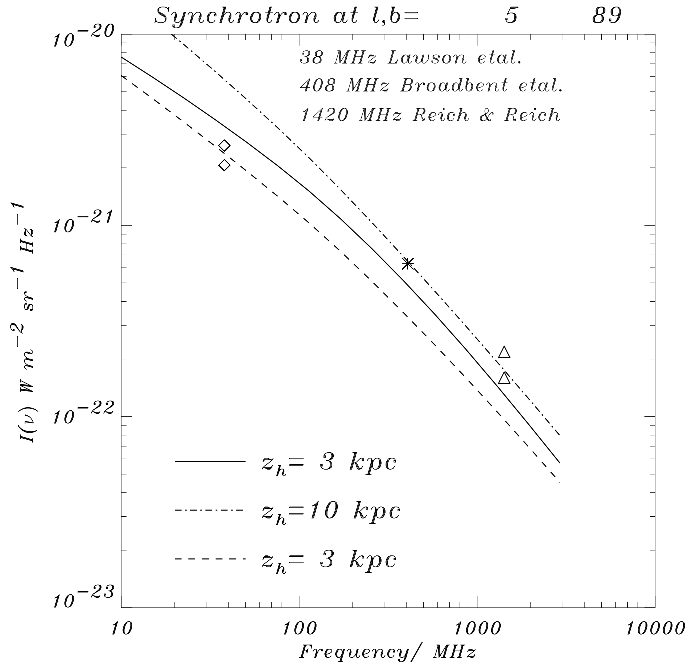

Fig. 18 . Synchrotron spectrum towards Galactic pole for the electron spectra shown in Fig 12 . Dashed and dashed-dot lines are for models with constant electron injection index -2.4. Dashed line: z_h = 3 kpc, D_o = 2 10^{28} cm^2 s^{-1} , dashed-dot line: z_h = 10 kpc, D_o = 5$10^{28}$ cm^2 s^{-1} . Full line: electron injection spectrum with break at 3 GeV, z_h = 3 kpc, D_o = 2 10^{28} cm^2 s^{-1} . The 408 MHz point is from the analysis of Broadbent et al. (1990); the 38 MHz points are obtained assuming a spectral index range of 0.5-0.6 (Lawson et al. (1987). The 1420 MHz values use the spectral index range 2.85-3.1 (Reich and Reich 1988).

9. Fine-tuning of the model

The models with a constant electron injection index -2.4 can reproduce *all* the data considered to within a factor 2; for the γ-ray spectrum covering 4 decades of energy this is already an interesting result. However the discrepancies between model and observations are very significant and sufficient to suggest some fine-tuning of the parameters. However this is not simple since improvement in one area often leads to a worse fit elsewhere. Adopting a flatter electron injection spectrum with γ= 2.2 instead of 2.4 would improve the fit to the low-frequency radio data but would disagree with the high-frequency radio index and also produce too few γ-rays below 30 MeV; in addition it would seriously overpredict the measured electron spectrum above 10 GeV. To obtain a better fit by adjusting the injection spectrum therefore requires a more complex model, for example with a break, with spectral index 2.2 below 3 GeV steepening to 2.6 above 3 GeV. The radio data (Section 8.5) indeed suggest a break in the electron spectrum at a few GeV. This would also allow us to fit the Ulysses electron flux at 9 GeV including a possible larger solar modulation factor mentioned in Section 8.3, to better fit and the balloon data above 50 GeV. Thus several completely independent lines of evidence point to a break in the electron injection spectrum and we therefore we conclude that this is the simplest way to achieve an improvement in the fit to all the data considered. The propagated spectrum for an injection spectrum of this kind, for z_h = 3 kpc and D=2$10^{28}$ cm^2 s^{-1} , is shown in Fig 12 , normalized now to agree with a 60% higher 9 GeV flux and to fit the observed spectrum in the 50 GeV - 1 TeV range. The corresponding non-thermal spectrum is shown in Fig 18 ; the observed steepening is reproduced better, although the radio data by themselves would suggest that an even large break is required.

Another parameter which can be optimized is the size of the halo; an intermediate halo model with z_h = 5 kpc is preferred since this is in better agreement with the γ-ray data as described in Section 8.4.2, and is consistent with studies of the 408 MHz emission (Phillipps et al. 1981; Beuermann et al. 1985). This model predicts a relatively large IC contribution to the γ-ray intensity at high latitudes and this may be the key to further progress.

The cosmic-ray source gradient could also be tuned to agree better with the γ-ray data but here it is better to await new EGRET analyses which take account of possible unresolved point-source populations which is the main uncertainty in the analysis (Strong and Mattox 1996) used here.

10. Prospects for future developments

Having demonstrated the practicality of the numerical method for a relatively simple case, we intend to extend it to include diffusive reacceleration and convection, and also to address the positron spectrum which will provide additional and valuable constraints on the models. The proton spectrum and He isotope spectra can also be addressed.

11. Conclusions

We have demonstrated that a numerical approach allows the generation of models of cosmic-ray propagation which include realistic elements of Galactic structure and which predict a wide range of observational material. It provides a powerful tool for future studies in this field and a basis for further development.

Despite the many observational constraints, there is still much freedom allowed in some physical attributes of the model, as shown by the fact that our two standard halo heights z_h =3 and 10 kpc can both be brought into approximately equal accord with the data with an optimum being at an intermediate value z_h = 5 kpc. A more detailed study of the high-latitude γ-ray

---

* Broadbent et al. (1989) investigated extreme forms of the electron spectrum which could produce the rapid change in the radio spectral slope.

sky with EGRET data could give more restrictive constraints in future.

A steepening in the electron injection spectrum from γ = 2.2 to 2.6 around a few GeV would simultaneously improve the fit to the radio, γ-ray and direct electron measurements, and therefore the evidence for such a break is a tentative conclusion of this paper. It is important to note that this break cannot be produced by propagation or energy losses, at least within the present model (which is highly constrained by the nucleon and other data).

The models reproduce the γ-ray data within a factor 2 over the range 1 MeV - 10 GeV, but the discrepancies are significant. Of particular relevance are the low-energy γ-ray predictions, which are now of sufficient accuracy to allow a critical confrontation with the emissivities measured by COMPTEL. The agreement is satisfactory within the γ-ray measurement errors. Above 1 GeV energies the predicted spectrum is systematically too low, but this well known discrepancy may have other origins (e.g. a flat-spectrum discrete source population).

The locally measured electron spectrum is well reproduced over the range 10 GeV - 1 TeV where solar modulation is small enough for a meaningful comparison. The low-energy spectrum as derived from the γ-ray data and propagation models is proving useful input to studies of cosmic-ray modulation in the heliosphere (Ferrando et al. 1996; Rastoin et al. 1996; Haasbroek et al. 1995). The possibility of a larger solar modulation at 10 GeV predicted by current models of the heliosphere can be accomodated provided there is a break in the electron injection spectrum as described above.

The non-thermal radio spectrum provides a useful constraint and demonstrates that our model produces the correct absolute intensity. The steepening of the slope around 408 MHz is again compatible a break in the electron injection spectrum round 3 GeV.

The inverse Compton γ-ray calculations should be the most accurate to date because of the model consistency with all the independent observational constraints, and a recalculation of the radiation field incorporating new mid- and far- IR information. This is important for studies of the extragalactic diffuse γ-ray emission.

12. Detailed results in electronic form

Since the detailed results of these calculations are 3D distributions in (R,z,E) or (l,b,E) which are large datasets to which other users may wish to have access, we will make these available in electronic form as FITS files. The data types are: interstellar radiation field U(R,z,ν), electron spectra I_e(R,z,E_e), γ-ray bremsstrahlung emissivity q(R,z,E_γ), inverse Compton skymaps I_{ics}(l,b,E_γ) and total γ-ray intensity skymaps I_γ(l,b,E_γ).

Access to these data and more information on this project, including all the programs, is available on the WWW site http://www.gamma.mpe-garching.mpg.de/∼aws/aws.html (or contact the author at aws@mpe-garching.mpg.de).

13. APPENDIX: Numerical method for solution of diffusive propagation with energy losses

The diffusive, convective and energy loss terms in equation (1) can all be finite-differenced for each dimension (R,z,E) in the form

$$\frac{\partial\psi_i}{\partial t} = \frac{\alpha_1\psi_{i-1} - \alpha_2\psi_i + \alpha_3\psi_{i+1}}{\Delta t} - \frac{\psi_i}{\tau} + q_i \qquad A1$$

where τ includes the inelastic and/or radiactive decay loss terms. All terms are functions of (R,z,E).

In the Crank-Nicolson implicit method (Press et al. 1992) the updating scheme is

$$\psi_i^{t+\Delta t} = \psi_i^t + \alpha_1\psi_{i-1}^{t+\Delta t} - \alpha_2\psi_i^{t+\Delta t} + \alpha_3\psi_{i+1}^{t+\Delta t} - \frac{\Delta t}{\tau}\psi_i^{t+\Delta t} + q_i\Delta t$$

The tridiagonal system of equations

$$-\alpha_1\psi_{i-1}^{t+\Delta t} + (1 + \alpha_2 + \frac{\Delta t}{\tau})\psi_i^{t+\Delta t} - \alpha_3\psi_{i+1}^{t+\Delta t} = \psi_i^t + q_i\Delta t$$

is solved for the $\psi_i^{t+\Delta t}$ by the standard method (Press et al. 1992).

The formulae for the coefficients in R, z and E are:

$$\left.\begin{aligned} \alpha_1^R &= R_- \\ \alpha_2^R &= (R_- + R_+) \\ \alpha_3^R &= R_+ \end{aligned}\right\} \quad \times \frac{2D\Delta t}{\Delta R(R_+^2 - R_-^2)}$$

where $R_- = R - \frac{\Delta R}{2}$, $R_+ = R + \frac{\Delta R}{2}$

$$\alpha_1^z = \frac{D\Delta t}{\Delta z^2} \qquad \alpha_2^z = 2\frac{D\Delta t}{\Delta z^2} \qquad \alpha_3^z = \frac{D\Delta t}{\Delta z^2}$$

$$\alpha_1^E = 0 \qquad \alpha_2^E = \frac{dE}{dt}\left(E\right)\frac{\Delta t}{\Delta E} \qquad \alpha_3^E = \frac{dE}{dt}\left(E + \Delta E\right)\frac{\Delta t}{\Delta E}$$

Note that for α^E we use 'upwind' differencing to enhance stability, which is possible since we have only energy *loss* terms.

The three spatial boundary conditions

$$\psi(R, z_h, E) = \psi(R, -z_h, E) = \psi(R_h, z, E) = 0$$

are imposed at each iteration. No boundary conditions are imposed or required at R = 0 or in E.

Since we have a 3-dimensional (R,z,E) problem we use 'operator splitting' to handle the implicit solution. We apply the implicit updating scheme alternately for the operator in each dimension in turn, replacing ψ_i by the updated values in each substep. $\frac{q_i}{3}$ and $\frac{1}{3\tau}$ are used instead of q_i, τ to account for the substeps. The method was found to be stable even for $\alpha >> 1$, and this property can be exploited to advantage (see below). The standard alternating direction implicit method (ADI), in which the full operator is used to update each dimension implicitly in turn, is more accurate but was found to be unstable for $\alpha > 1$; this is a disadvantage when treating problems with many timescales, but can be used to generate an accurate solution from an approximation generated by the non-ADI method.

A check for convergence is performed by computing the timescale $\frac{\psi}{\partial\psi/\partial t}$ from equation A1 and requiring that this be large compared to all diffusive and energy loss timescales. The main problem in applying the method in practice is the wide range of time-scales, especially for the electron case, ranging from 10^4 years for energy losses to 10^9 years for diffusion around 1 GeV in a large halo. Use of a time step Δt appropropriate to the smallest time-scales guarantees a reliable solution but requires a prohibitively large number of steps to reach the long time-scales. The following technique was found to work very well: start with a large Δt appropriate for the longest scales, and iterate until a stable solution is obtained. This solution is then accurate only for cells with $\alpha << 1$; for other cells the solution is stable but inaccurate. Then reduce Δt by a factor (0.8 was adopted) and continue the solution. This process is repeated until $\alpha << 1$ for all cells; then the solution is accurate everywhere. It is found that the inaccurate parts of the solution quickly decay as soon as the condition $\alpha < 1$ is reached for a cell. As soon as all cells satisfy $\alpha < 1$ the solution is continued with the ADI method to obtain maximum accuracy. A typical run starts with Δt = 10^6 years and ends with Δt = 10^2 years, performing 100 iterations per Δt. In this way it is possible to obtain reliable solutions in a reasonable computer resources, although the CPU required is still considerable.

The program is written in the IDL language; a FORTRAN implementation which would be many time faster, is planned. The code can be obtained as described in Section 12.

ACKNOWLEDGEMENTS

This work has benefitted from many disussions with V. Dogiel and M. Pohl. I also thank P. Ferrando and M. Potgieter for discussions concerning the Ulysses electron results and heliospheric propagation.

REFERENCES

Bertsch D. et al., 1994 Ap. J. **416**, 587

Beuermann, K., Kanbach, G., Berkhuijsen, E.M. 1985, A&A. **153**, 17

Boulanger, F., Désert F.X., 1992, in 'The Infrared and Submillimetre Sky after COBE', M. Signore and C. Dupraz (eds), p.263, Kluwer Academic Publishers, Dordrecht

Bloemen, H., 1985 A&A. **145**, 391

Bloemen, H., Deul, E.R., Thaddeus, P. 1990, A&A. **233**, 437

Bloemen, H., Dogiel, V.A., Dorman, V.L., Ptuskin, V.S. 1993, A&A, **267**, 372

Blumenthal G R, Gould R J, 1970, Rev. Mod. Phys. **42**, 237

Broadbent, A., Haslam, C.G.T., Osborne, J.L. 1989, MNRAS **237**, 381

Broadbent, A., Haslam, C.G.T., Osborne, J.L. 1990, Proc. 21st ICRC, Adelaide, **3**, 229

Bronfmann L et al., 1988, ApJ **324**, 248

Chi, X., Wolfendale, A.W. 1991, J. Phys. G. **17**, 987

Cordes J.M. et al. 1991, Nature **354**, 121

Cox P, Krügel E., Mezger P G, 1986, A&A, **155**, 380

Cox P, Mezger P G, 1989, Astron. Astr. Rev. **1**, 49

Désert F-X, Boulanger F, Puget J L 1990, A&A, **237**, 215

Digel, S.W. et al. 1996, ApJ **406**, 609

Engelmann J J et al., 1990, A&A, **233**, 96

Ferrando P et al., 1988, Phys. Rev. C **37**, 1490

Ferrando P et al., 1996, A&A *in press*

Ginzburg, V.L., 1979, 'Theoretical Physics and Astrophysics' , Pergamon Press

Golden, R.L. et al. 1984, ApJ, **287**, 622

Golden, R.L. et al. 1994 ApJ **436**, 769

Gordon M A., Burton, W B., 1976, ApJ **208**, 346

Gupta M, Webber W R, 1989, ApJ **340**, 1124

Haasbroek, L.J., Potgieter, M.S., Webber, W.R., 1995, Proc. 24th ICRC, Rome, **4**, 706

Heiles, C. 1996, ApJ **462**, 316

Heinbach, U., Simon, M., 1995, ApJ **441**, 209

Hunter, S.D. et al. 1995, Proc. 24th ICRC, Rome, **2**, 182

Hunter, S.D. et al. 1996, A&A Supp, *in press*

Kappadath S.C. et al. 1996, A&A Supp, *in press*

Kent S M, Dame T M, Fazio G., 1991, ApJ **378**, 131

Koch H W, Motz J W., 1959, Rev. Mod. Phys. **31**, 920

Kodaira, K. 1974, PASJ, **26**, 255

Lawson K D et al., 1987, MNRAS **225**, 307

Lerche I., Schlickeiser R 1981 ApJSupp, **47**, 33

Lerche I., Schlickeiser R 1982a A&A, **107**, 148

Lerche I., Schlickeiser R 1982b MNRAS, **201**, 1041

Lukaskiak A et al. 1994 ApJ **423**, 426

Mannheim K, Schlickeiser R., 1994, A&A, **286**, 983

Mathis J S., Rumpl W., Nordsiek K.H., 1977, ApJ **217**, 425

Mathis J S, Mezger P, Panagia N, 1983, A&A, **128**, 212

Matsumoto T. et al. 1988, ApJ **329**, 567

Nishimura, J. et al. 1995, Proc. 24th ICRC, **3**, 29

Owens, A.J. and Jokipii, J.R., 1977, ApJ **215, 677**

Pacholczyk, A.G., 1970, 'Radio Astrophysics', W.H. Freeman and Company, San Francisco

Phillipps, S. et al. 1981, A&A, **103**, 405

Press, W. H. et al., 1992, 'Numerical Recipes in FORTRAN', 2nd Edition, Cambridge University Press.

Purcell W. et al., 1995, Proc. 24th ICRC, **2**, 211

Purcell W. et al., 1996, A&A Supp *in press*

Rand R J, Lyne, A.G., 1994, MNRAS **268**, 497

Rastoin, C. et al. 1996, A&A, **307**, 981

Reich P., Reich W., 1988 A&A, **196**, 211

Reynolds R J., 1989, ApJ **339**, L29

Reynolds, S.P., 1991, Proc. AIP Conf **264**, 'Particle Acceleration in Cosmic Plasmas', ed. Zank G.P. and Gaisser T.K., p. 409

Skibo, J.G., Ramaty, R., Purcell W.R. 1995, Proc. 24th ICRC, **2**, 219
Skibo, J.G., Ramaty, R., Purcell W.R. 1996, A&A Supp *in press*
Sodrowski T J et al., 1994, ApJ **428**, 638
Stecker F. W. 1988, ApJ, *Cosmic Gamma Rays, Neutrinos and Related Astrophysics*, ed Shapiro M. M. and Wefel J.P., (Dordrecht:Reidel), 85
Strong, A.W. (1996) Sp. Sc. Rev. **76**, 205
Strong, A.W., Mattox, J.R. (1996), A&A, **308**, L21
Strong, A. W. et al. 1988, A&A, **207**, 1
Strong, A. W. et al. 1994, A&A, **292**, 82
Strong, A. W. et al. 1995, Proc. 24th ICRC, **2**, 234
Strong, A.W., Youssefi G, 1995, Proc. 24th ICRC, **3**, 48
Strong, A.W. et al. 1996, A&A Supp *in press*
Taira T et al. 1993 Proc 23rd ICRC, **2**, 128
van der Kruit P C., 1986, A&A, **157**, 230
van der Walt, D.J., 1990, Astrophys. Sp. Sci. **168**, 23
Webber, W.R. 1983, in 'Composition of Origin of Cosmic Rays', ed. Shapiro, M. M., pub. D. Reidel, p. 83
Webber, W.R., Kish J C, Schreier D A 1990a, Phys. Rev. C. **41**, 520
Webber, W.R., Kish J C, Schreier D A 1990b, Phys. Rev. C. **41**, 533
Webber, W.R., Kish J C, Schreier D A 1990c, Phys. Rev. C. **41**, 547
Webber, W.R., Lee, M.A., Gupta, M. 1992, ApJ, **390**, 96
Webber, W.R. et al. 1996, ApJ **457**, 435
Yamasaki, N.Y. et al. 1996, A&A Supp *in press*
Youssefi G, Strong A. W.,1991 Proc 22nd ICRC **1**, 129